Available online at www.sciencedirect.com
SCIENCE DIRECT®
International Journal of Heat and Mass Transfer 48 (2005) 4354–4366
International Journal of HEAT and MASS TRANSFER
www.elsevier.com/locate/ijhmt

Transient vaporization and burning in dense droplet arrays

Randall T. Imaoka, William A. Sirignano *

Department of Mechanical and Aerospace Engineering, University of California, Irvine 3202 Engineering Gateway, Irvine, CA 92697-3975, United States

Received 14 April 2005; received in revised form 21 May 2005
Available online 28 July 2005

Abstract

Three-dimensional droplet-array combustion with an unsteady liquid-phase and a quasi-steady gas-phase is studied computationally by a generalized approach using a mass-flux potential function. Symmetric and asymmetric droplet arrays with non-uniform droplet size and non-uniform spacing are considered. Burning rates are computed and correlated with the number of droplets, an average droplet size, and an average spacing for the array through one similarity parameter for arrays as large as 1000 droplets. Total array vaporization rates are found to be maximized at a specific droplet number density that depends on liquid volume within the array. An unsteady liquid-phase model with either a uniform or a radially varying temperature distribution is coupled with the quasi-steady gas-phase solution for decane, heptane, and methanol fuels. Droplet interactions and liquid-phase heating have been shown to almost double the lifetime when compared to an isolated droplet. Depending on fuel type, initial temperature, and array geometry, droplets may initially burn with individual flames, transition to a single group flame, and transition back to individual flames as vaporization progresses. In most cases, group combustion occurs upon ignition and is the dominant mode of combustion.

Keywords: Dense sprays; Group combustion

1. Introduction

Fuel droplet vaporization and burning rates are known to be influenced by the presence of neighboring droplets. Labowsky transformed the governing equations into Laplace's equation for a potential function and studied vaporization without Stefan convection [1], vaporization with Stefan convection [2], and combustion [3]. Two-drop arrays were studied analytically by Umemura et al. [4,5], Brzustowski et al. [6], Twardus and Brzustowski [7], and numerically by Sivasankaran et al. [8]. Marberry et al. [9] considered up to 8-droplets in a manner similar to the method-of-images, with an approximation made to account for the effects of neighboring droplets. Elperin and Krasovitov [10] solved Laplace's equation using a similar method, but used higher order corrections to account for the effects of neighboring droplets. More recently, Imaoka and Sirignano [11] solved the three-dimensional Laplace's equation using finite-difference computations for symmetric arrays of up to 216 droplets. A correlation for array vaporization rates was given in terms of a similarity

* Corresponding author. Tel.: +1 949 824 3700; fax: +1 949 824 3773.
E-mail addresses: rimaoka@uci.edu (R.T. Imaoka), sirignan@uci.edu (W.A. Sirignano).

0017-9310/$ - see front matter © 2005 Elsevier Ltd. All rights reserved.
doi:10.1016/j.ijheatmasstransfer.2005.05.012

Nomenclature

a	droplet radius
B	transfer number
c_p	constant pressure specific heat
d	inter-droplet spacing
D	binary diffusion coefficient
h	specific enthalpy
L	latent heat of vaporization
L_{eff}	effective latent heat of vaporization
$\dot{m}$	mass vaporization rate
N	number of droplets
$\dot{q}$	magnitude of heat flux
Q	heating value per unit mass of fuel
r	radial coordinate
t	time
T	temperature
V	volume
$\vec{V}$	mass-averaged velocity vector
Y	mass fraction
Greek symbols	
α	thermal diffusivity
η	normalized vaporization rate
λ	thermal conductivity
ν	stoichiometric fuel to oxidizer mass ratio
ξ	similarity parameter
ρ	mixture density
Φ	normalized potential function
Φ_{B}	bifurcation contour
Φ_{F}	flame contour
Subscripts	
0	initial value
∞	ambient value
A	array
avg	average
eq	equivalent value
F	fuel
i	inner
iso	isolated droplet
j	the jth droplet
l	liquid
max	maximum
min	minimum
o	outer
O	oxidizer
opt	optimal
S	surface value
WB	wet-bulb

parameter incorporating array spacing and the number of droplets. Quasi-steady flame shapes and flame positions were also obtained.

The transformation of the governing equations to a three-dimensional Laplace's equation is not restricted to symmetric, mono-sized, or uniformly-spaced arrays. However, literature on quantitative variations of individual droplet sizes or locations within an array has been limited to three-drop arrays. Studies of larger asymmetric droplet arrays have not been performed. Although the image methods in [3,9,10] are all capable of dealing with more "realistic" droplet arrays, they will encounter difficulty when relative droplet spacing is small, and/or the number of droplets is large [11]. In contrast, for a fixed number of droplets, a finite-difference solution converges faster for dense arrays than sparse arrays (due to fewer nodes), making it superior for problems involving strong droplet interactions. In this paper, solutions for burning rates in dense asymmetric arrays are obtained using both finite-difference computations and, when possible, the method-of-images. Flame shapes and locations, however, can be computed more easily by finite-differencing than by the image method.

Despite the extensive literature available on droplet-array burning, research on unsteady droplet-array burning with liquid-phase heating has not been documented. Law [12] and Law and Sirignano [13] discussed unsteady droplet burning for a single, isolated droplet using different liquid-phase heating models. In this paper, a quasi-steady gas phase is coupled with an unsteady liquid phase for decane, heptane, and methanol arrays of up to eight droplets. The effects of ambient temperature and ambient oxidizer mass fraction are noted. Conduction-limit and infinite-liquid-conductivity [14] models are implemented in the liquid-phase, and compared to vaporization without liquid heating. Droplet size, liquid temperature distributions, flame shapes, and flame locations are obtained over the lifetime of the arrays.

2. Gas-phase problem formulation

The assumptions and gas-phase analysis follow the generalized formulation in [15]. The potential function Φ governing mass flux in the gas-phase satisfies Laplace's equation and the following boundary conditions.

$$\nabla^2\Phi = 0 \qquad \begin{cases} \Phi = 0 & \text{on droplet surfaces} \\ \Phi = 1 & \text{far from the droplets.} \end{cases} \tag{1}$$

The solution to (1) with the desired droplet geometry yields the effect of droplet interactions. Enthalpy,

composition, flame contour location, and the quantity $\overline{\rho D}$ are obtained through the simultaneous solution of the following equations:

$$(1+B)^{\overline{\rho D}\int_0^{\Phi}\frac{\mathrm{d}\Phi'}{\lambda/c_p}} = 1+\frac{h-h_S+vQY_O}{L_{\mathrm{eff}}} = 1+\frac{Y_F-Y_{FS}-vY_O}{Y_{FS}-1} \tag{2}$$

$$\overline{\rho D} = \left(\int_0^1 \frac{\mathrm{d}\Phi'}{\lambda/c_p}\right)^{-1} \tag{3}$$

$$\frac{\ln(1-Y_{FS})}{\ln(1+B)} = -\overline{\rho D}\int_0^{\Phi_F}\frac{\mathrm{d}\Phi'}{\lambda/c_p} \tag{4}$$

With a unitary Lewis number, the quantities ρD and λ/c_p are equal and will be used interchangeably. The Spalding transfer number B is computed as

$$B = \frac{h_\infty - h_S + vQY_{O\infty}}{L_{\mathrm{eff}}} = \frac{vY_{O\infty}+Y_{FS}}{1-Y_{FS}}, \tag{5}$$

$$L_{\mathrm{eff}} = L + \frac{\dot{q}_l}{|\rho\vec{V}|_S}. \tag{6}$$

Vaporization rates are obtained by integrating the mass flux over the surface of the droplets. For the jth droplet,

$$\dot{m}_j = \overline{\rho D}\ln(1+B)\int\int \nabla\Phi\cdot\mathrm{d}\vec{A}_j. \tag{7}$$

A normalized vaporization rate η_j is defined as the actual vaporization rate of the jth droplet divided by the vaporization rate of an isolated droplet vaporizing in an identical environment.

$$\eta_j = \frac{\dot{m}_j}{\dot{m}_{\mathrm{iso}}} = \frac{1}{4\pi a_j}\int\int \nabla\Phi\cdot\mathrm{d}\vec{A}_j \tag{8}$$

A normalized array vaporization rate η_A is computed as the average of η_j over all droplets in the array. Eqs. (1)–(8) are taken directly from [15], where (2)–(6) are independent of the droplet array size and configuration. In contrast, Eqs. (1) and (8) depend only on geometry and not on fuel type or boundary conditions. Therefore, solutions for the scalar variables and transport properties become one-dimensional in terms of Φ. The three-dimensional analysis is only necessary in solving Eq. (1). Computing actual vaporization rates from (7) will require a specified geometry, boundary conditions, and fuel type.

Solutions for the normalized potential function Φ are obtained by solving Laplace's equation in the gas-phase. A finite-difference scheme, with a composite grid consisting of spherical-polar and Cartesian coordinate systems is used. Vaporization rates are obtained by numerically integrating $\nabla\Phi$ over the droplet surfaces. For arrays with few droplets and/or arrays with large droplet spacing, solutions are obtained using the method-of-images. Details regarding the numerical scheme, boundary conditions, and criteria for convergence and feasibility of a method-of-images solution can be found in [11].

In the literature pertaining to multiple droplet arrays, vaporization rates are usually normalized as in Eq. (8). Therefore, specification of fuel type, boundary conditions, or any gas-phase transport properties were not required for the non-dimensional vaporization rates. Such analyses only assess the geometrical aspects of droplet array burning by solving Eqs. (1) and (8). Furthermore, only mono-sized arrays were considered for more than three droplets. The normalized vaporization rate given by Eq. (8) does not depend on thermophysical properties and has the same value for constant properties as for variable properties. Flame contours prior to [11] had only been presented for two-drop arrays. The use of a constant value for ρD has been shown to significantly overestimate flame stand-off distances [15]. In this paper, quasi-steady vaporization rates in asymmetric arrays with variable droplet-size are obtained, and correlated with previous findings for symmetric, mono-sized arrays. Using an average droplet size and average droplet spacing, vaporization rates are shown to be optimized with a specific number of droplets. Changes in flame topology due to inter-droplet spacing and variations in droplet radii are demonstrated. Unsteady vaporization with and without liquid-phase heating is studied for decane, heptane, and methanol droplets. Time-varying flame contours are presented. Throughout this paper, variable (temperature and composition dependent) gas-phase properties are used.

3. Quasi-steady vaporization rates of asymmetric arrays

3.1. Effect of droplet spacing

In order to study the effects of droplet spacing, droplet radii, and array configuration on the total array burning rate, the effects of each parameter are analyzed individually. To find the effects of droplet spacing, an N-droplet array with constant droplet radius is stretched initially in one coordinate direction, then simultaneously in two coordinate directions. Calculations were performed for more than 50 different droplet arrays of 9, 27, and 64 droplets, as well as droplets arranged in a 30-drop pyramid to study the effects of asymmetry. 27- and 64-drop arrays are cubic or rectangular arrays with three and four droplets along an edge of the rectangular volume. A 9-drop array consists of an 8-drop array with one additional droplet at the center of the array. The arrays were elongated in various increments so that the largest droplet spacing exceeded the smallest droplet spacing by at least a factor of 3; however, the droplet spacing was uniform in each of the three directions within the array. Droplet spacings varied between 3 and 50

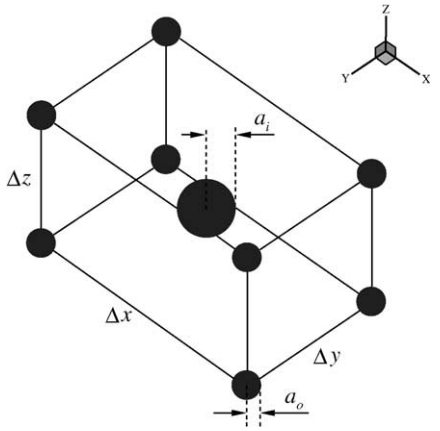

Fig. 1. The droplet arrangement and spacing for a 9-drop rectangular array with variable radii and non-uniform spacing.

radii. The configuration of a rectangular 9-drop array is shown in Fig. 1.

Previous results from [11] have shown that, in a 125-drop mono-sized cubic array with $d/a = 3$, the outermost droplet will vaporize more than 5000 times faster than the central droplet of the array. However, while not previously mentioned, the induced Stefan velocity leaving the array might further enhance the burning rates of the outer droplets, making the factor of 5000 a conservative estimate. At that same spacing but with 1000 droplets, the difference is more than a factor of 10^7. Since the current problem formulation permits only normal velocities at the droplet surfaces, the effects of very strong blowing velocities from the inner droplets creating boundary layers over the outer droplets are not included in the analysis. The orders of magnitude difference in vaporization rates of the inner droplets versus the outer droplets supports the neglect of this effect. Results from [11] also indicate that vaporization rates for symmetric droplet arrays with uniform droplet radii and spacing correlate well with a similarity parameter ξ given by,

$$\xi(d/a, N) = \frac{d}{aN^{0.72}}. \tag{9}$$

Uniform arrays consisting of 8–216 droplets were studied in [11], but more recent unpublished results show good correlations with up to 1000 droplets. A relationship between the array vaporization rate η_A and the similarity parameter ξ was found as,

$$\eta_A(\xi) = 1 - \frac{1}{1 + 0.725671\,\xi^{0.971716}}. \tag{10}$$

The first-term on the RHS in the above equation represents the normalized array vaporization rate in the absence of droplet interactions. The denominator of the second term, through the similarity parameter ξ, embeds implicitly the effect of the interactions.

To utilize Eqs. (9) and (10) for droplet arrays with non-uniform spacing, the average center-to-center distance to be used in Eq. (9) should be computed as

$$d = \frac{V_A^{1/3}}{N^{1/3} - 1}, \tag{11}$$

where V_A is the array volume enclosed by a surface drawn through the line of centers of the outermost droplets. The numerical value of d obtained using (11) represents the spacing that would be obtained if the array were reconfigured into a symmetric array with uniform spacing. As a result, (11) applied to symmetric, cubic arrays with uniform spacing and three planes of symmetry will yield the correct spacing. Normalized vaporization rates for the aforementioned 9-, 27-, 30-, and 64-drop arrays with non-uniform spacing are shown as calculated from Eqs. (9) and (11) in Fig. 2a. The agreement between the vaporization data and Eq. (10) shown in

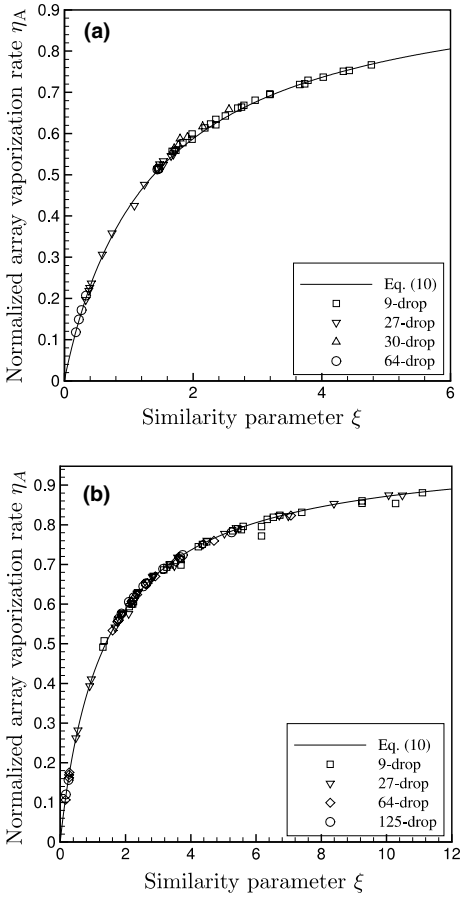

Fig. 2. Normalized array vaporization rates versus the similarity parameter ξ. (a) Non-uniform spacing and (b) variations in droplet radii.

Fig. 2a can be attributed to the parameter d_{max}/d_{min}. When d_{max}/d_{min} is larger than ~3, and d is computed with Eq. (11), vaporization rates may not be accurately predicted by (10). This disagreement arises when a three-dimensional array is stretched substantially in one or two directions, and affects both uniform and non-uniform arrays. Therefore, vaporization rates for arrays consisting of droplets in a line or in a plane are not predicted well. If only a few droplets within the array have exceptional spacing but the overall external geometry of the array is still somewhat three-dimensional, (11) might still be valid since a local extremum of spacing will have a small effect on average. Furthermore, the validity of Eq. (11) does not depend strongly on the positions of individual droplets within the array and therefore, does not consider the details of any non-uniformity in droplet spacing within the array.

3.2. Effect of droplet radii

To isolate and identify the effects of droplet radii variations, asymmetric or non-uniformly spaced arrays were not considered simultaneously with radii variations. Cubic arrays of 9, 27, 64, and 125 droplets, were separated into inner and outer regions, with droplet radii varying between these regions. The inner regions in each of the arrays consisted of 1, 1, 8, and 27 droplets, respectively. The ratio of inner droplet radius, a_i, to outer droplet radius, a_o, was varied from 0.25 to 10.0 for more than 90 different droplet arrays with $3 < d/a_{max} < 50$. Since individual-droplet vaporization rates will be largest for the outermost droplets of an array [11], emphasis was placed on arrays with $a_i/a_o > 1$.

Eqs. (9) and (10) both require information on droplet radius. For arrays with non-constant droplet radii, a characteristic radius, a_{avg}, was computed as a linear average of the individual-droplet radii

$$a_{avg} = \frac{1}{N}\sum_{j=1}^{N} a_j. \tag{12}$$

For a finite number of droplets with infinite droplet spacing, the total vaporization rate of the array will be $4\pi\overline{\rho D}\ln(1+B)$ multiplied by the sum of the droplet radii. Therefore, it is not surprising that a good correlation is achieved with a linear average. By varying a_i/a_o with different array geometries and taking the linear average of the droplet radii, the vaporization results compared well with previous results for mono-sized arrays. These results and Eq. (10) are shown versus ξ in Fig. 2b. A linear average of the droplet radii gives good agreement with Eq. (10) except for 9-drop arrays with large values of a_i/a_o. However, emphasis is placed on larger, more realistic arrays, where a better correlation was achieved. The error between computed data and Eq. (10) for most cases was <1% and did not exceed 5%.

3.3. Maximum vaporization rate

Although the normalized array vaporization rate η_A gives a good indication of the relative reduction in vaporization rate due to interactions, the effects of droplet spacing and droplet radii variation on the actual vaporization rate are not immediately obvious due to the normalization. From Eqs. (9) and (10), η_A is a monotonically increasing function of ξ. Therefore, for an array of mono-sized droplets, an increase in η_A could result from either an increase in droplet spacing or a decrease in the total number of droplets. However, both of these parameter changes directly affect the ratio of the volume of fuel to the total volume of the array. In an array of droplets occupying a volume V_A with a total liquid volume V_l, it is worthwhile to study the vaporization rates of various arrays for a fixed value of V_l/V_A.

A $3\times3\times3$, 27-drop cubic array with uniform droplet size and a center-to-center spacing of 7.5 droplet radii is used as the datum. A $4\times4\times4$, 64-drop array is constructed with mono-sized droplets but with the same V_l/V_A. This geometry change will result in a 6.3% increase in the vaporization rate. However, a $5\times\ 5\times5$, 125-drop array with the same V_l/V_A yields only a 5.7% increase in the burning rate. These results show that vaporization rates are maximized at specific droplet number densities.

By definition of the normalized array vaporization rate for a mono-sized droplet array and from Eq. (10)

$$\eta_A = \frac{\dot{m}_A}{4\pi a N\overline{\rho D}\ln(1+B)} = 1 - \frac{1}{1+0.725671\,\xi^{0.971716}}. \tag{13}$$

In (13), ξ can be expressed as

$$\xi = \frac{\left(\frac{4\pi V_A N}{3V_l}\right)^{1/3}}{(N^{1/3}-1)N^{0.72}} \tag{14}$$

by utilizing Eq. (11) and by expressing average droplet radius in terms of N and V_l. Eq. (12) then is bypassed in determining the average radius. Substitution into (13) and again expressing a in terms of V_l yields the non-dimensional relation

$$\frac{\dot{m}_A}{\overline{\rho D}\ln(1+B)V_A^{1/3}} = (4\pi N)^{2/3}\left(\frac{3V_l}{V_A}\right)^{1/3}\left(1-\frac{1}{1+0.725671\left(\frac{\left(\frac{4\pi V_A N}{3V_l}\right)^{1/3}}{(N^{1/3}-1)N^{0.72}}\right)^{0.971716}}\right). \tag{15}$$

Dividing (15) through by $V_A^{2/3}$ and multiplying by $\overline{\rho D}\ln(1+B)$, gives the vaporization rate per unit volume of the array

$$\frac{\dot{m}_A}{V_A} = \overline{\rho D}\ln(1+B)\left(\frac{4\pi N}{V_A}\right)^{2/3}\left(\frac{3V_l}{V_A}\right)^{1/3} \times \left(1 - \frac{1}{1+0.725671\left(\frac{\left(\frac{4\pi V_A N}{3V_l}\right)^{1/3}}{(N^{1/3}-1)N^{0.72}}\right)^{0.971716}}\right). \quad (16)$$

Eq. (15) is evaluated in Fig. 3 with V_l/V_A as a parameter. Again, the normalization process for the vaporization rate in Eqs. (15) and (16) hides the dependence on the thermophysical properties. The results indicate that there exists a droplet number density at which the vaporization rate is maximized for a fixed value of V_l/V_A. While it might intuitively seem that, for a given V_l/V_A, a higher vaporization rate per unit array volume will always be possible by increasing N and thereby increasing liquid surface area, the results show that this is only true until a critical droplet number. For an array with few droplets, the increase in total surface area that will result from dividing the liquid into smaller droplets will increase the vaporization rate. However, beyond this critical droplet number, additional droplets will effectively reduce the inter-droplet spacing so that a reduction in vaporization rates is observed. As $N \to \infty$, the RHS of (15) approaches zero asymptotically. Note that increasing V_A for fixed V_l and N is essentially increasing the relative droplet spacing, which will result in improved vaporization rates. If Eq. (16) is used to find the optimal droplet number density, the analysis will provide the number of mono-sized droplets in the volume of the array that would maximize vaporization rate. The size of these droplets should be computed so that the total liquid volume satisfies the desired V_l/V_A. Although the present work has shown that droplet size variations can be handled by a linear average of the radii from Eq. (12), note that $a_{avg}^3 \leqslant \frac{1}{N}\sum_{j=1}^{N} a_j^3$. Therefore, using Eq. (12) to remove droplet size variations will, in general, not conserve liquid volume or the parameter V_l/V_A. Droplet-size variations are still possible as long as the liquid volume is conserved. However, conserving liquid volume with non-uniform droplet radii will result in an increase in the linear average of droplet radii a_{avg} as the radii variation increases. This will cause a reduction in ξ and consequently η_A. Note that Eqs. (13) and (15), and therefore the plots in Figs. 2a, b, and 3 are normalized so that they universally apply to any liquid fuel. The results would be modified if transient heating of the liquid interior occurs, as will be discussed later.

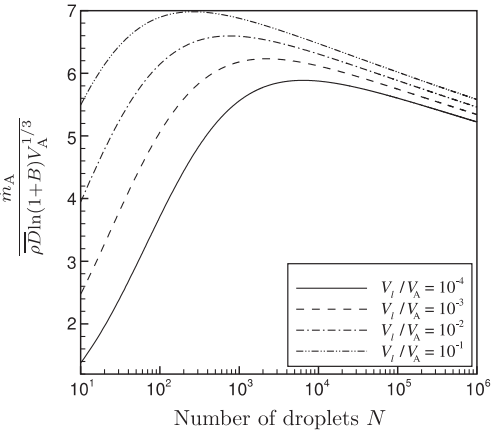

Fig. 3. The non-dimensional vaporization rate from Eq. (15) versus N for different values of V_l/V_A.

The optimal number of droplets, N_{opt}, can be found in terms of V_l/V_A through differentiation of Eq. (15). The roots of the resulting equation are found with V_l/V_A as a parameter. The results yield an almost linear relationship between $\ln(N_{opt})$ and $\ln(V_l/V_A)$. Fitting a power curve to the results yields the following expression for N_{opt}.

$$N_{opt} = 11.377\left(\frac{V_l}{V_A}\right)^{-0.6047}. \quad (17)$$

Eq. (17) shows that the optimal number of droplets depends only on the parameter V_l/V_A. Therefore, an increase in the array volume, coupled with an equivalent increase in liquid volume, will have no effect on N_{opt}. For typical hydrocarbon combustion at near stoichiometric conditions and moderate pressures, V_l/V_A will be $\sim 10^{-3}$, indicating that the optimal number of mono-sized, uniformly spaced droplets is approximately 800. In most practical spray applications, $N \gg 800$.

4. Quasi-steady flame location

The solution for Φ directly yields information on flame shape and location. In the limit of infinite kinetic rate, flames will lie on the constant Φ surface computed from Eq. (4). Results from previous work on symmetric, mono-sized droplet arrays with uniform spacing [11] are relevant here. Constant Φ surfaces govern the flame shape and location, and are obtained throughout the gas-phase for different droplet geometries. In any array with $N \geqslant 2$, there exists a range of values of Φ for which contour surfaces engulf more than one droplet. The lowest Φ values represent contours that surround only individual droplets. Depending on fuel type and boundary conditions, transition between individual-droplet burning, partial group combustion, and complete group combustion can be dictated by the relative droplet spacing.

Exact flame shapes and locations for a given droplet array can be obtained upon specification of the temperature and composition of the ambience and at all droplet surfaces. Satisfaction of Eqs. (5) and (6) with $\dot{q}_l = 0$ ensures the droplets are at their wet-bulb temperatures. Previous work [11] has shown that, for droplets burning at wet-bulb temperatures, individual-droplet flames are very unlikely. Furthermore, it was shown that, in most realistic arrays, flame stand-off distance was larger than the array dimensions and a flame surrounding the array was nearly spherical. As a result, the droplet array burned approximately as a single, isolated droplet of equivalent radius $a_{eq} = aN\eta_A$. Although quasi-steady, single-droplet burning analyses tend to overestimate flame-standoff distances compared with experimental findings, variable properties have been shown to yield more accurate results [15,16]. In [11], changes in flame topology were illustrated by varying droplet surface temperature. However, the proper determination of surface temperature requires an unsteady liquid-phase analysis and will be discussed in Section 6. Changes in flame topology are possible with droplets at wet-bulb temperatures by varying droplet size and spacing.

Two 5-drop arrays, each with one central droplet and four peripheral droplets, are arranged such that all droplets lie in a plane, as indicated in Fig. 4a–c. Each of the four peripheral droplets are positioned at equal distances from the inner droplet. The ambience is at one atmosphere pressure with $T_\infty = 298$ K and $Y_{O\infty} = 0.5$. From Eq. (4), and the determination of variable properties [15], the flame surface corresponds to Φ values of 0.7963 and 0.9078 for methanol and decane, respectively, with droplet surface temperatures of 331.62 K and 437.96 K. The flame surfaces are shown for the 5-drop, planar arrays with inner/outer droplet ratios a_i/a_o of 1, 2, and 20. The results are shown in Fig. 4a–c. for the plane of symmetry intersecting all droplet centers with the methanol flame as the solid line and the decane flame as the dashed line.

Although 5-drop planar arrays were not used to correlate data in Fig. 2a and b, their analysis illustrates the effects of droplet size and spacing on flame positions. Using the previously calculated Φ_F values, Fig. 4a–c show that the decane flame always has a larger standoff distance than a methanol flame. In Fig. 4a, both fuels burn with a single flame. In Fig. 4b, only methanol burns with individual flames and in Fig. 4c, with $a_i/a_o = 20$, both fuels burn with individual flames. While a droplet size differential of this magnitude could exist, it is unlikely any array would consist of only five droplets. Increasing N would make individual flames more difficult to observe.

Droplet spacing in a mono-sized array can also produce changes in flame topology. Using the same 5-drop array, the distance between the central drop and two of the four outer drops is increased, effectively stretching the array as indicated in Fig. 5a and b. Flame shapes are evaluated with different degrees of stretching, d_{max}/d_{min}. With $d_{max}/d_{min} = 1$, the flames behave as in Fig. 4a. Fig. 5a and b show the droplet geometry and

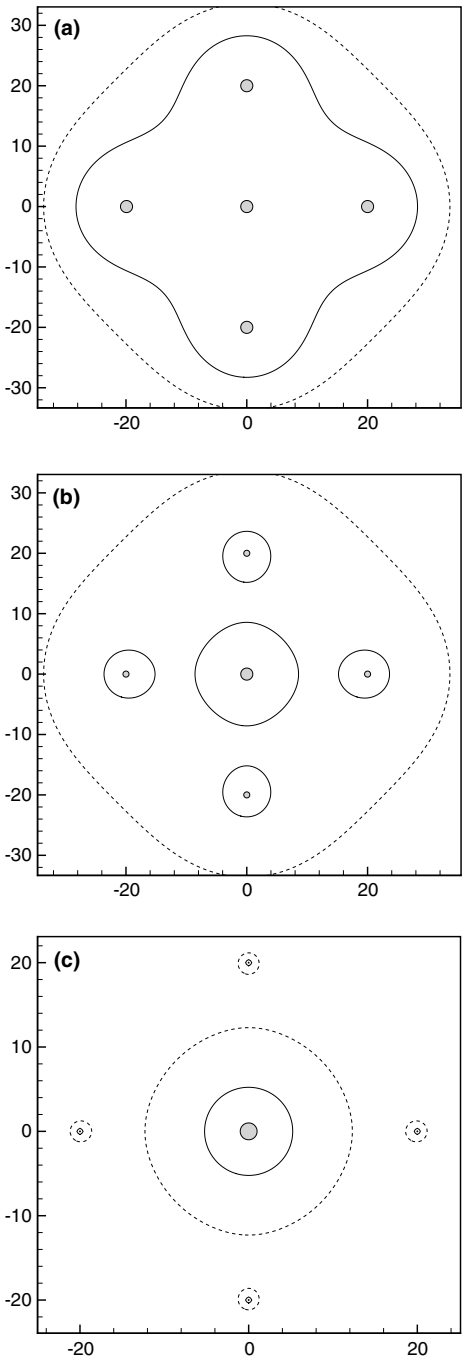

Fig. 4. Flame locations for methanol (solid) and decane (dashed) droplets in a planar 5-drop array with spacing $d/a_i = 20$: (a) $a_i/a_o = 1$; (b) $a_i/a_o = 2$ and (c) $a_i/a_o = 20$.

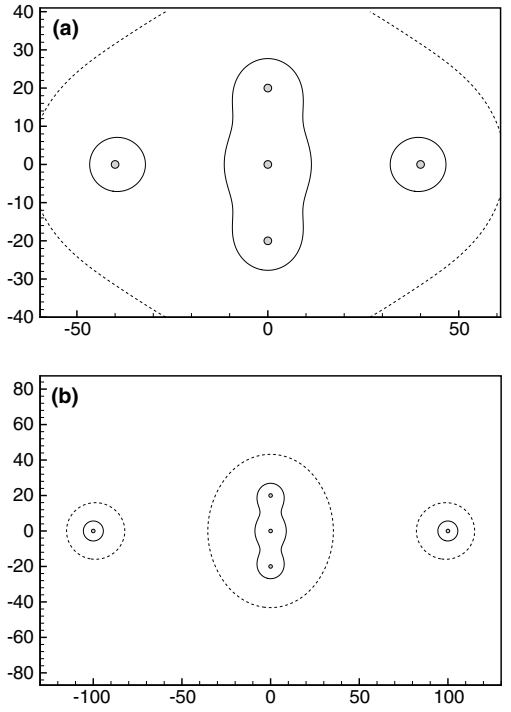

Fig. 5. Flame locations for methanol (solid) and decane (dashed) droplets in a planar, mono-sized 5-drop array with $d_{\min}/a = 20$: (a) $d_{\max}/d_{\min} = 2$ and (b) $d_{\max}/d_{\min} = 5$.

flame shapes in the plane of symmetry for $d_{\max}/d_{\min}$ values of 2 and 5. The solid and dashed lines give the flame positions of methanol and decane, respectively. The figures indicate that non-uniformly varying droplet spacing can also lead to individual-droplet flames. When $d_{\max}/d_{\min} = 1$, complete group combustion occurs for both fuels. As the array is stretched, partial group combustion is attainable with methanol at $d_{\max}/d_{\min} = 2$, and with decane at $d_{\max}/d_{\min} = 5$. Even at $d_{\max}/d_{\min} = 5$, individual-droplet flames are not possible for the three adjacent droplets in the center of the array. An increase in vertical droplet separation is necessary to observe individual-droplet flames for all five droplets.

It has been shown that individual-droplet flames, partial group combustion, and complete group combustion can occur as a result of changes in relative droplet sizes and spacing while burning at wet-bulb temperatures. In arrays with more than five droplets, complete group combustion is more likely. For example, all of the decane, heptane, and methanol droplet arrays studied with more than nine droplets would burn with a single flame surrounding the array. To observe individual-droplet flames for droplets at wet-bulb temperatures in larger arrays will require a much larger inter-droplet spacing, or, the majority of the droplets must be orders of magnitude smaller than a few of the larger droplets. Still, such a situation may exist in actual sprays as the combustion process is near completion. Changes in flame shape due to increases in inter-droplet spacing and surface temperatures are shown in Section 7.

5. Vaporization at wet-bulb temperature with time varying droplet radii

In this case, $\dot{q}_l = 0$ in Eq. (6) so that $L_{\text{eff}} = L$ and the relation in Eq. (5) prescribes the constant wet-bulb surface temperature and the wet-bulb value of B. The reduction in vaporization rates due to droplet interactions will increase droplet lifetimes in multiple droplet arrays. From Eqs. (7) and (8), the vaporization rate of the jth droplet is given by

$$\dot{m}_j = \dot{m}_{\text{iso}}\eta_j = 4\pi a\overline{\rho D}\ln(1+B_{\text{WB}})\eta_j = -\rho_l\frac{\mathrm{d}}{\mathrm{d}t}\left(\frac{4\pi a_j^3}{3}\right). \tag{18}$$

The isolated droplet lifetime, t_{iso}, is given by

$$t_{\text{iso}} = \frac{\rho_l a_0^2}{2\overline{\rho D}\ln(1+B_{\text{WB}})}. \tag{19}$$

Introducing the dimensionless variables $\hat{t} = t/t_{\text{iso}}$ and $\hat{a} = a/a_0$, Eq. (18) can be rewritten as

$$\frac{\mathrm{d}\hat{a}_j^2}{\mathrm{d}\hat{t}} = -\eta_j. \tag{20}$$

A fourth order Runge–Kutta scheme is used to integrate Eq. (20) over the lifetime of the droplet. The number of time steps over one droplet lifetime was of order 10^4. The non-dimensional scheme makes Eq. (20) independent of the fuel choice.

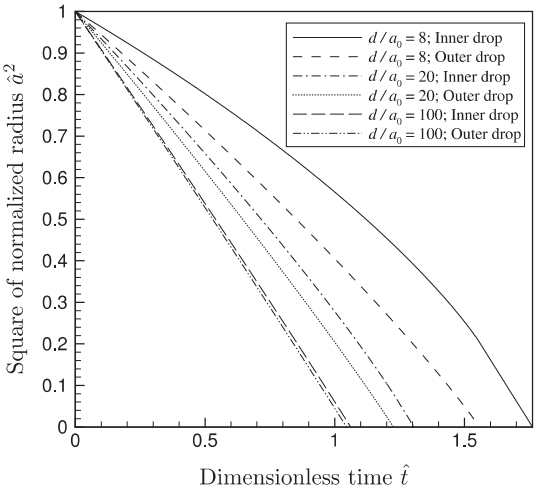

Fig. 6. Square of normalized droplet radius versus time for the inner and outer droplets of a 9-drop cubic array without liquid heating.

When droplets do not experience the same interactions, individual droplet lifetimes will vary. The square of the normalized droplet radius is shown versus time in Fig. 6 for the central and outer droplets of an initially mono-sized, 9-drop, cubic array with $d/a_0 = 8$, 20, and 100. These normalized results hide the effects of thermophysical properties. With an initial spacing of eight droplet radii, the inner droplet of the 9-drop array has a lifetime ~75% greater than an isolated droplet. In all cases, the eight outer droplets will have shorter lifetimes than the inner drop. This effect diminishes as droplet spacing is increased. As $d/a_0 \to \infty$, interactions become negligible, $\hat{a}^2$ becomes linear as predicted by the *d*-squared law, and lifetimes are given by Eq. (19). Upon vaporization of the outer drops, the surface area of the single remaining drop decreases linearly in time.

6. Unsteady vaporization with liquid-phase heating

Now, liquid-phase heating is included in the analysis by solving the diffusion equation within the droplets. It is assumed that liquid temperature varies only radially within any droplet. Furthermore, droplet interactions must be identical for each droplet in the array. Uniform surface temperatures with $\dot{q}_l$ varying over the droplet surfaces is a reasonable approximation. Variations in surface tension with temperature would create an internal convection that would tend to remove temperature gradients along the droplet surface [14]. With these assumptions, a 1D diffusion equation for the liquid-phase is coupled with the quasi-steady gas-phase to incorporate liquid-phase heating in equal-interaction arrays.

The spherically symmetric diffusion equation, with constant liquid thermal diffusivity α_l

$$\frac{\partial T}{\partial t} = \frac{\alpha_l}{r^2}\frac{\partial}{\partial r}\left(r^2\frac{\partial T}{\partial r}\right), \tag{21}$$

is made non-dimensional using the variables $\hat{t} = t/t_{iso}$, $\hat{r} = r/a$, and $\hat{a} = a/a_0$. The isolated droplet lifetime t_{iso} is given by Eq. (19). Note that the droplet radius a is now time-varying. Incorporating these dimensionless variables, Eq. (21) becomes

$$\frac{\partial T}{\partial \hat{t}} = \frac{\alpha_l t_{iso}}{(a_0\hat{a})^2}\frac{\partial^2 T}{\partial \hat{r}^2} + \left(\frac{2\alpha_l t_{iso}}{(a_0\hat{a})^2\hat{r}} + \frac{\hat{r}}{2\hat{a}^2}\frac{\mathrm{d}\hat{a}^2}{\mathrm{d}\hat{t}}\right)\frac{\partial T}{\partial \hat{r}}. \tag{22}$$

The transformation to $\hat{r}$ removes the moving boundary associated with droplet surface regression. A modification is made to Eq. (20) to compensate for the droplets not being at the wet-bulb temperature.

$$\frac{\mathrm{d}\hat{a}^2}{\mathrm{d}\hat{t}} = -\frac{\ln(1+B)}{\ln(1+B_{WB})}\eta_A \tag{23}$$

The time-varying Spalding transfer number B depends on the instantaneous heat flux into the liquid and the surface temperature, which is now lower than the wet-bulb temperature. B should be computed with the second relationship in Eq. (5). Eqs. (5) and (6) together with a phase-equilibrium relation determine $\dot{q}_l$ as a function of surface temperature; this conductive heat flux provides the droplet surface boundary condition.

$$\left.\frac{\partial T}{\partial \hat{r}}\right|_{\hat{r}=1} = \frac{\overline{\rho D}}{\lambda_l}\ln(1+B)\left(\frac{h_\infty - h_S + vQY_{O\infty}}{B} - L\right)\eta_A. \tag{24}$$

Eq. (24) is the non-linear relationship between the droplet surface temperature (through B, h_S, $\overline{\rho D}$, and λ_l), and the temperature gradient at the droplet surface. Due to spherical symmetry, zero gradient exists at the droplet center. An average heat flux $\bar{\dot{q}}_l$ defines the rate of droplet heating.

$$\bar{\dot{q}}_l = \frac{1}{4\pi a^2}\int\int \dot{q}_l \cdot \mathrm{d}\vec{A} = \frac{\lambda_l}{a}\left.\frac{\partial T}{\partial \hat{r}}\right|_{\hat{r}=1} \tag{25}$$

This analysis assumes negligible internal liquid circulation and will therefore be termed a *conduction-limit* model, as in previous work [13]. As $\lambda_l \to \infty$, temperatures will be time-varying but spatially uniform throughout the droplet. This will be referred to as an *infinite-conductivity* model [14]. Solutions to Eq. (22) and the surface boundary condition (24) are obtained using a Crank–Nicholson scheme, with a minimum of 100 radial nodes in the liquid and $\sim 10^4$ time steps over the droplet lifetime. Eq. (23) is integrated using a fourth order Runge–Kutta scheme with η_A computed either numerically or with the method-of-images when possible. Decane, heptane, and methanol fuels were considered, and all droplets started with a uniform temperature distribution. The values for $\overline{\rho D}$ used in (24) were computed with the correlations in [15]. Unlike combustion at wet-bulb temperatures, the incorporation of liquid-phase heating does not permit the results to apply universally to all fuels.

Decane droplet interactions were shown in Fig. 6 to reduce vaporization rates and increase droplet lifetimes for droplets at wet-bulb temperatures. Liquid-phase heating further reduces droplet burning rates. Normalized radius squared with and without droplet heating is shown versus dimensionless time in Fig. 7a–c for 8-droplet cubic arrays with $T_0 = 298$ K and initial spacings of 6, 10, and 50 radii. Decane surface temperatures and liquid-heating rates are shown for one isolated droplet lifetime in Fig. 8a and b.

As droplet spacing decreases, liquid-phase heating persists over a larger fraction of the droplet lifetime. Fig. 7a–c demonstrate the influence of droplet spacing on burning rates for these fuels when liquid-phase heating is included. Liquid-phase heating increases isolated droplet lifetimes by 19.2%, 9.7%, and 2.4%, for decane, heptane, and methanol, respectively. For eight droplets

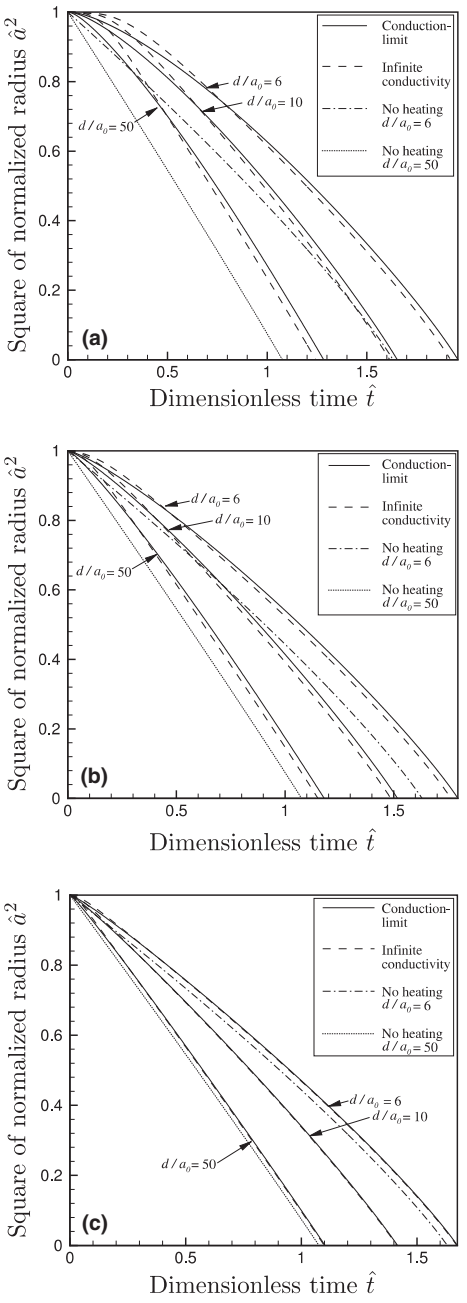

Fig. 7. Radius squared versus time for 8-drop, cubic arrays with $T_0 = 298$ K, $T_\infty = 298$ K, and $Y_{O\infty} = 0.231$. (a) Decane; (b) heptane and (c) methanol.

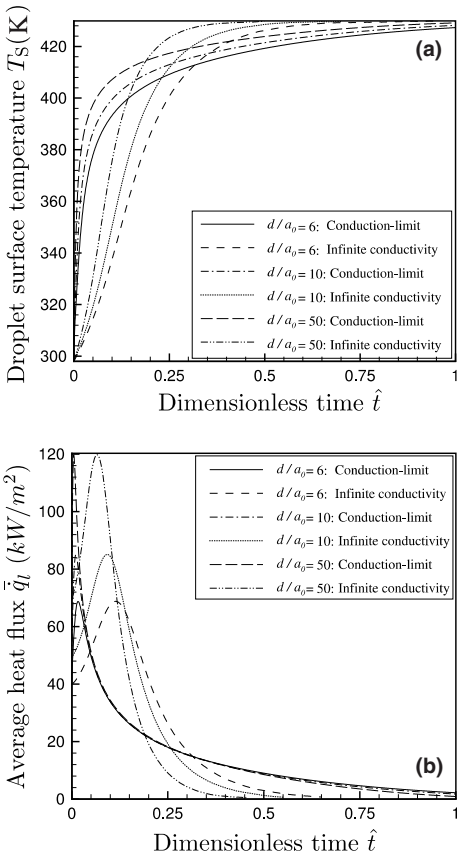

Fig. 8. Temperature (a) and average conductive heat flux (b) at the droplet surface versus time for eight decane drops with $T_0 = 298$ K, $T_\infty = 298$ K, and $Y_{O\infty} = 0.231$.

with $d/a_0 = 6$, droplet lifetimes are increased by factors of 1.96, 1.8, and 1.67 for the three fuels. With decane, a decrease in initial spacing from 10 to 6 radii results in a 18% increase in droplet lifetime. This sensitivity to droplet interactions for small droplet spacing comes from the reduction in both mass and heat transfer at the droplet surfaces through Eqs. (23) and (24). The reduced transport at the droplet surfaces due to droplet interactions is dictated by η_A, which yields the reduction in the Nusselt and Sherwood numbers relative to an isolated droplet at wet-bulb temperature. Note the smaller initial heat flux for denser arrays in Fig. 8b. The correction for the droplets not being at wet-bulb temperature is contained in B. Interactions would have a greater effect if the current array were larger than eight droplets and/or the initial spacing were reduced. Droplet interactions will be even greater in actual sprays.

The two liquid-phase models predict different droplet lifetimes [14]. With the conduction-limit model, surface temperatures increase rapidly in the presence of a flame, while the droplet core temperature remains largely unaffected. These higher surface temperatures, while advantageous for increasing vaporization rates, decrease the rate of liquid-phase heating. Now, the increased heating rate from the infinite-conductivity model will lead to a greater surface temperature and burning rate as combustion proceeds, resulting in shorter lifetimes. Due to lower wet-bulb temperatures of methanol, liquid-heating does not hinder burning rates as substantially as with the

other fuels. This is demonstrated in Fig. 7c, where the difference between the two models, and with no liquid-heating, is less dramatic.

Fig. 8b indicates that the rate of liquid-phase heating increases initially upon ignition for both liquid-phase models with decane droplets. This is caused by the significant increase in $\overline{\rho D} = \overline{\lambda/c_p}$ with increasing surface temperature [15]. During the initial period, the sum of the energy used to vaporize the droplet and that used to heat the liquid interior increases, providing the increased rate of droplet heating despite a decreasing temperature difference between the ambient gas and the droplet surface. The increase in the rate of liquid-phase heating occurs over a shorter time interval with the conduction-limit model because surface temperature and composition respond faster with this model.

Normalized radius squared versus time is shown in Fig. 9 for decane droplets with different ambient oxidizer mass fractions using the conduction-limit model.

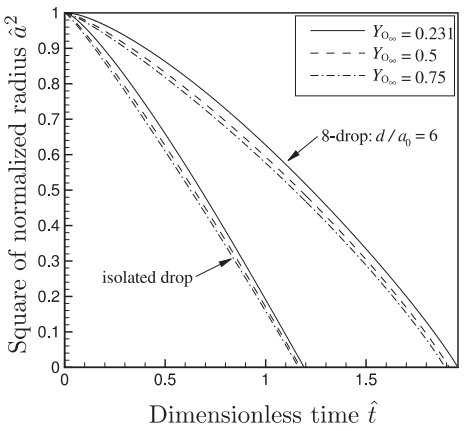

Fig. 9. Normalized radius squared versus time for decane drops with $T_0 = 298$ K and $T_\infty = 298$ K. Conduction-limit model.

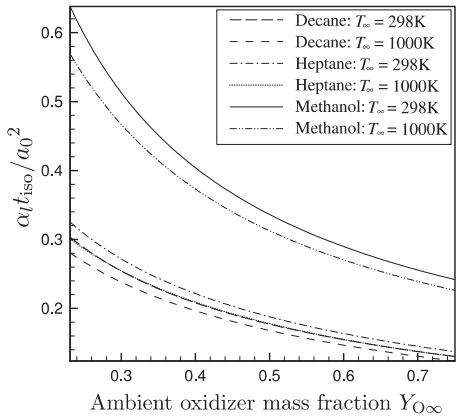

Fig. 10. Dimensionless isolated droplet lifetimes are shown versus ambient oxidizer mass fraction.

Dimensionless isolated droplet lifetimes are shown in Fig. 10 versus ambient oxidizer mass fraction for the three fuels with $T_\infty = 298$ K and $T_\infty = 1000$ K. A higher ambient oxidizer concentration lowers isolated droplet lifetimes through $\overline{\rho D}$. Fig. 9 further shows that, with liquid-heating, normalized lifetimes are also reduced with increasing $Y_{O\infty}$. Heptane and methanol followed the same trend, but were less sensitive to changes in $Y_{O\infty}$. Previous findings [15] show that ambient temperature T_∞ had less of an effect on gas-phase properties than $Y_{O\infty}$. Therefore, while isolated droplet lifetimes will vary, normalized droplet lifetimes and flame location will not depend strongly on ambient temperature.

7. Unsteady flame position

The flame contour surface is determined by Eq. (4). In [11], flames were found to depend strongly on droplet surface temperature, which affected flame topology. With liquid-heating, changes in surface composition resulting from increasing liquid temperatures can cause a transition from individual-droplet flames to group combustion. Fig. 11 shows this transition for a planar, 4-drop array with decane droplets, at an initial temperature of 298 K and initial spacing of five radii. Flame contour values Φ_F and the contour value associated with bifurcation, Φ_B, are shown in Fig. 12 versus instantaneous droplet spacing d/a for decane, heptane, and methanol, with the same initial geometry as in Fig. 11. Time has been removed from the abscissa to enable comparison between the fuels. Note that Φ_B is only a function of array geometry. Individual flames will be present if $\Phi_F < \Phi_B$. The Φ_F values used in the figures were obtained using the correlations provided in [15].

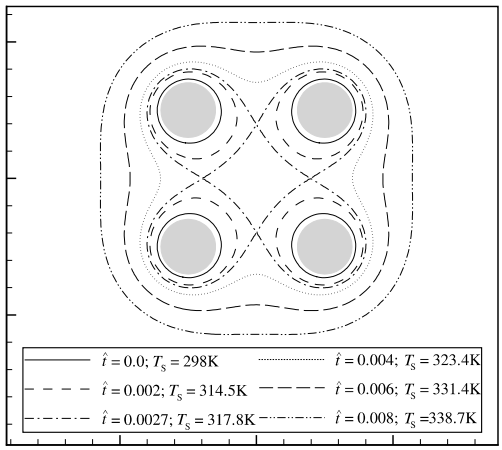

Fig. 11. Flame contours for a 4-drop, decane array with $d/a_0 = 5$, $T_0 = 298$ K, $T_\infty = 298$ K, and $Y_{O\infty} = 0.231$. Conduction-limit model.

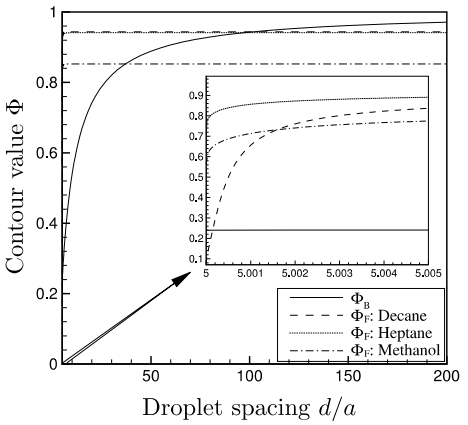

Fig. 12. Change in flame shape versus instantaneous droplet spacing for various fuels in a 4-drop array with d/a_0=5, $T_0 = 298$ K, $T_\infty = 298$ K, and $Y_{O\infty} = 0.231$. Conduction-limit model.

The transition to group combustion shown in Fig. 11 occurs at less than 0.2% of the droplet lifetime. Consequently, group combustion is present over most of the array lifetime. As indicated by the inset in Fig. 12, heptane and methanol droplets with the same array geometry and ambience will burn as a group upon ignition. For arrays with non-uniform droplet interactions, multiple values of Φ_B may exist.

While only decane droplets initially burn with individual-flames, all three fuels will burn with a single flame for most of their lifetime, and transition to individual-flames toward the end of their lifetime. The effective increase in spacing caused by the reduction in droplet size leads to isolated droplet behavior. However, transition to individual-flames occurs after the majority of the liquid volume has vaporized, and may have little effect on the overall combustion process. As previously mentioned, the individual-droplet flames encountered with decane upon ignition exist initially for less than 0.2% of the droplet lifetime. Since we do not analyze the ignition process in proper detail, this early behavior might not be well described.

8. Conclusions

Three-dimensional droplet-array combustion with liquid-phase heating and variable thermophysical properties has been studied computationally with a generalized approach using a mass-flux potential function. Methods for computing an average droplet size and spacing enable quasi-steady vaporization rates to correlate well with existing data for symmetric, mono-sized arrays with uniform spacing. Vaporization rates are maximized at specific droplet number densities that depend only on the ratio of liquid volume to total array volume. Based on these findings, which do not address situations with forced convection, typical droplet burning applications would benefit from a reduction in droplet number density and an increase in droplet size at fixed liquid volume. An unsteady liquid-phase model with either a uniform or a radially varying temperature distribution in the liquid is coupled with the quasi-steady gas-phase solution for decane, heptane, and methanol droplet arrays. Droplet interactions are shown to have an effect on vaporization even in the absence of liquid heating. With droplet interactions, liquid-phase heating has been shown to nearly double the lifetime of a single, isolated droplet. Changes in flame shapes and flame locations are demonstrated at wet-bulb temperatures through variations in array geometry, and by surface temperature changes due to transient liquid-phase heating. Although individual-droplet flames are possible at the initiation and termination of combustion, for most practical arrays, a single flame will exist over most of the lifetime.

References

[1] M. Labowsky, The effects of nearest neighbor interactions on the evaporation rate of cloud particles, Chem. Eng. Sci. 31 (1976) 803–813.
[2] M. Labowsky, A formalism for calculating the evaporation rates of rapidly evaporating interacting particles, Combust. Sci. Technol. 18 (1978) 145–151.
[3] M. Labowsky, Calculation of the burning rates of interacting fuel droplets, Combust. Sci. Technol. 22 (1980) 217–226.
[4] A. Umemura, S. Ogawa, N. Oshima, Analysis of the interaction between two burning droplets, Combust. Flame 41 (1981) 45–55.
[5] A. Umemura, S. Ogawa, N. Oshima, Analysis of the interaction between two burning fuel droplets with different sizes, Combust. Flame 43 (1981) 111–119.
[6] T. Brzustowski, E.M. Twardus, S. Wojcicki, A. Sobiesiak, Interaction of two burning fuel droplets of arbitrary size, AIAA J. 17 (1979) 1234–1242.
[7] E.M. Twardus, T.A. Brzustowski, The interaction between two burning fuel droplets, in: Fifth International Symposium on Combustion Processes, Krakow, Poland, vol. 8, 1977.
[8] K. Sivasankaran, K.N. Seetharamu, R. Natarajan, Numerical investigation of the interference effects between two burning fuel spheres, Int. J. Heat Mass Transfer 39 (18) (1996) 3949–3957.
[9] M. Marberry, A.K. Ray, K. Leung, Effect of multiple particle interactions on burning droplets, Combust. Flame 57 (1984) 237–245.
[10] T. Elperin, B. Krasovitov, Analysis of evaporation and combustion of random clusters of droplets by a modified method of expansion into irreducible multipoles, Atomization Sprays 4 (1994) 79–97.
[11] R.T. Imaoka, W.A. Sirignano, Vaporization and combustion in three-dimensional droplet arrays, Proceedings of the Combustion Institute 30 (2005) 1981–1989.

[12] C.K. Law, Unsteady droplet combustion with droplet heating, Combust. Flame 26 (1976) 17–22.
[13] C.K. Law, W.A. Sirignano, Unsteady droplet combustion with droplet heating—II. Conduction-limit, Combust. Flame 28 (1977) 175–186.
[14] W.A. Sirignano, Fluid Dynamics and Transport of Droplets and Sprays, Cambridge University Press, New York, 1999.
[15] R.T. Imaoka, W.A. Sirignano, A generalized analysis for liquid-fuel vaporization and burning, Int. J. Heat Mass Transfer, in press, doi:10.1016/j.ijheatmasstransfer.2005.05.018.
[16] B.N. Raghunandan, H.S. Mukunda, The problem of liquid droplet combustion—a reexamination, Combust. Flame 30 (1977) 71–84.